

Modeling Stellar Interiors
of Zero Age Main Sequence Stars

By
Anthony P. Rasca

Carroll College MT
April 2007

Project Advisor: Kelly S. Cline, Assistant Professor
Department of Mathematics, Engineering,
and Computer Science

CORETTE LIBRARY
CARROLL COLLEGE

This thesis for honors recognition has been approved for the

Department of Mathematics .



Director

4/3/07

Date

Anthony M. Szpilka

Reader

4/3/07

Date



Reader

4/3/07

Date

TABLE OF CONTENTS

Abstract	ii
Introduction: Studying the Unreachable	1
Equations of Stellar Structure	2
Assumptions for a Simple Model: Density as a Constant	10
Assumptions for a Simple Model: Linear Density	17
Conclusions	21
Appendix A: Constant Density Data	24
Appendix B: Linear Density Data	30
Works Cited	34

ABSTRACT

Studying aspects of nature unable to be measured or observed has been a problem in the field of astronomy. This study looks at the interiors of zero-age main sequence (ZAMS) stars and how they are studied, despite being several light-years away or more, by means of mathematical modeling. We introduce the equations of stellar structure key to establishing a model for the interior. Our assumptions were based on how density behaves in the interiors, which include constant and linear density change with respect to stellar radii. We used observational data from a range of spectral types to compare to our models. Stellar interiors according to the constant density model have decreasing core density, pressure and energy generation with respect to solar mass, which was expected to increase with increasing stellar mass. As predicted, core temperature and total luminosity increase sharply with increasing stellar mass and the total luminosity matches closely with the observational data for each spectral class. The linear density model actually gives less accurate results for total luminosity, making our first model better for calculating luminosity. All core conditions for each star increased, but density and pressure still dropped with respect to increasing stellar mass. With this information and the fact that our results were more accurate with low-mass stars, we conclude that density must change in more complex ways for high-mass stars with a steep gradient near the core. Such results point out the importance of using precise numerical methods in modeling stellar interiors.

INTRODUCTION: STUDYING THE UNREACHABLE

Much of the science we deal with is based on objects we can collect and study in a laboratory or out in the field. Natural scientists such as biologists, geologists, chemists, and physicists use these observations to understand how the world and everything on it works. We know how the bodies of various animals function because biologists have closely studied their anatomy and behavior; geologists use rocks and other pieces of the earth's crust to reveal its history. On a more basic level, chemists and physicists do laboratory experiments with chemicals and particles to learn how material works on a molecular or subatomic level. Being able to study a piece of the world up close is crucial to unlocking its secrets.

What if we cannot visit or bring the object to be studied to us? What if it's not even part of this world? Imagine trying to study something so far, that its light took thousand, millions, or even billions of years to reach us. We can't realistically study anything in the universe up close when it's located so far away. Most of the tangible science is only located on earth, which is infinitesimally small compared to the rest of the universe.

Getting around observational limitations takes using the little amount of information we do know to build a model. Scientific and mathematical modeling is extremely useful in studying the intangible areas of both the natural and social worlds. They can be use to predict oil prices, model the spread of a disease, or determine the effects of a meteor impact. On an astronomical level, everything is still subject to the

same physical principles we see applied to earth and its close surroundings. We can use this information to build a model of unreachable objects, particularly other stellar bodies.

Stars make up most of the observable matter in the universe, yet we can't simply travel to one to see what's on the inside or how it functions. Even our closest stellar neighbor hides its details beneath the blinding surface. The information we do know comes from the light stars send across the universe. From the light, we can use its color (spectral type), brightness (apparent luminosity), and movement in the sky (parallax) to determine its mass, temperature, absolute luminosity, and chemical composition. Stars are made up of materials which we are familiar with on earth, namely atomic hydrogen. Using stellar surface conditions and mathematical relationships for how matter behaves at various temperatures and pressures, we can build a stellar model to show how the interior is structured and how it functions.

EQUATIONS OF STELLAR STRUCTURE

From our limited observations, we can tell that stars are massive and generate a lot of energy given off in the form of light and heat. We want to know how states such as temperature, pressure, and mass change as we dig in from the surface to the center of the star. For most stars, the surface temperature and brightness change very little over a short period of time (Hansen 1). This implies a balance of various states within the star, including pressure, mass, and energy. The formulas describing how these states must

change between each layer of material, or *shell*, with respect to the distance r from the star's center are known as the equations of stellar structure*.

The balance of pressure, commonly referred to as hydrostatic equilibrium, deals with the downward force of gravity per area canceling out with the pressure in the opposite or *outward* direction. Hydrostatic equilibrium uses the opposing forces to keep the pieces of mass in one location. Taking into account cancellation, the pressure P , in Pascals, and gravitational force F_g , in Newtons, are easily related,

$$-\frac{F_g}{A} = P, \quad \text{Eq. 1}$$

where A , in m^2 , is the area which the mass is pressing down on. According to Newton's law of gravity,

$$F_g = -\frac{GM_r m}{r^2}, \quad \text{Eq. 2}$$

where G is the gravitational constant $6.67 \times 10^{-11} \text{ N}\cdot\text{m}^2\cdot\text{kg}^{-2}$, M_r is the mass in kg contained within the distance r , in meters, and m is the other mass interacting with M_r . We are concerned with the pressure at all points a particular distance r away from the center. Our m turns into the mass dm of an infinitely thin spherical shell with thickness dr . The thin shell equation for a change in mass assumes the area A on the inside is the same as on the outside of the shell,

$$dm = A\rho \cdot dr, \quad \text{Eq. 3}$$

with ρ as the density, in $\text{kg}\cdot\text{m}^{-3}$, at r . For a gravitational force difference dF_g , the mass difference dm is needed in Eq. 2 to form

* All equations in this section can be found in exact or similar form in several astronomy textbooks such as Carroll and Ostlie (1996).

$$dF_g = \frac{GM_r}{r^2} A \rho \cdot dr \quad \text{Eq. 4}$$

Substituting dF_g and the pressure difference dP into **Eq. 1** (remember that A is constant with respect to dr), we get

$$-\frac{GM_r A \rho \cdot dr}{Ar^2} = dP \quad \text{Eq. 5}$$

Canceling A and dividing both sides by dr gives us the equation of hydrostatic equilibrium,

$$\frac{dP}{dr} = -\frac{GM_r \rho}{r^2} \quad \text{Eq. 6}$$

With hydrostatic equilibrium and a known surface pressure, we can use **Eq. 6** to integrate towards the center and determine the structure for interior pressure.

Mass conservation also needs to be taken into consideration. The mass dM_r of a given thin shell, representing the change in mass across dr , is simply the product of the volume and density. Our mass equation is actually the same as **Eq. 3**, but substituting in $A = 4\pi r^2$,

$$dM_r = 4\pi r^2 \rho \cdot dr \quad \text{Eq. 7}$$

and thus giving us the mass conservation equation,

$$\frac{dM_r}{dr} = 4\pi r^2 \rho \quad \text{Eq. 8}$$

If we assume a uniform sphere, integrating both sides of **Eq. 7** from $r = 0$ to $r = R_*$, the stellar radius, we should get the total mass M_{R_*} :

$$M_{R_*} = \int_0^{R_*} 4\pi r^2 dr = \frac{4}{3} \pi r^3 \Big|_0^{R_*} \quad \text{Eq. 9}$$

$$M_{R_*} = \frac{4}{3}\pi R_*^3 \rho - \frac{4}{3}\pi 0^3 \rho = \frac{4}{3}\pi R_*^3 \rho = M_* \quad \text{Eq. 10}$$

Of course, we cannot assume density will be constant throughout the star, which is why we need to use the **Eq. 8** and the local density to calculate changes in the mass with respect to radius.

The amount of energy throughout the star needs to remain locally constant to keep stability. The energy generated L_r (in W) with the shell material is equal to the nuclear energy generation ϵ (in $\text{W}\cdot\text{kg}^{-1}$) times the available mass described in **Eq. 7**:

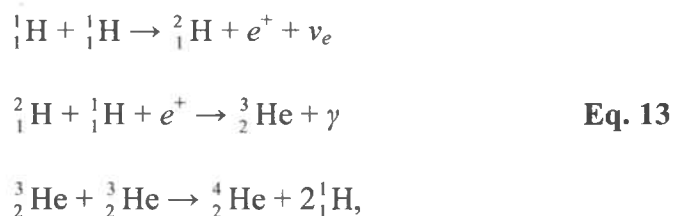
$$dL_r = 4\pi r^2 \rho \cdot dr \cdot \epsilon . \quad \text{Eq. 11}$$

By dividing both sides of **Eq. 11** by dr , we get the equation for energy conservation:

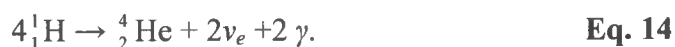
$$\frac{dL_r}{dr} = 4\pi r^2 \rho \cdot \epsilon \quad \text{Eq. 12}$$

Determining ϵ requires knowing about the nuclear reactions occurring that generate the energy

Through research done in nuclear physics, physicists have been able to study how different materials behave under various pressures and temperatures. When conditions are right, elements such as hydrogen and helium, smash together to produce a heavier element from two or more lighter atoms and produce a large output of energy in a process called nuclear fusion. The primary method of energy production for atomic hydrogen under high pressure and temperature is the proton-proton chain (p-p). The p-p chain consists of three independent reactions:



where ${}^{1+a}_1\text{H}$ and ${}^{2+a}_2\text{He}$ denote hydrogen and helium particles, respectively, containing a neutrons, e^+ is a positron (positively-charged electron antiparticle), ν_e is neutrino (lepton particle of almost no rest mass), and γ is a gamma ray (high-energy photon). The net reaction comes to be



The positrons that existed only between reactions were a result of ending with more neutrons than at the beginning. Two of the initial four protons shed a neutrino and their positive charge in the form of positrons to become neutrons. Since the positrons are antiparticles of electrons, the ones produced undergo annihilation with the electrons and become pure energy in the form of gamma rays.

Two additional p-p chains exist, known as PP II and PP III. PP II takes the ${}^3_2\text{He}$ produced in the second step of **Eq. 13** and instead of fusing them together to form ${}^4_2\text{He} + 2 {}^1_1\text{H}$, each reacts with an existing ${}^4_2\text{He}$ atom to begin a new chain. It forms beryllium and then lithium, which fissions back to become ${}^4_2\text{He}$. PP III takes abandoned beryllium atoms from the PP II chain and fuses with ${}^1_1\text{H}$ to generate boron, and then to ${}^4_2\text{He}$. Since not every ${}^3_2\text{He}$ from PP I (**Eq. 13**) is available for PP II, PP II is less common, and even less for PP III. ${}^3_2\text{He}$ falls into PP II only 31% of the time and beryllium is captured by PP III only 0.3% of the time (Carroll 344). The energy generating from all three p-p chains is summed up in the equation

$$\epsilon_{p-p} = 2.38 \times 10^2 \rho X^2 T_6^{-2/3} e^{-33.80 T_6^{-1/3}} \quad \text{Eq. 15}$$

in $\text{J}\cdot\text{kg}^{-1}\cdot\text{s}^{-1}$, as presented in Carroll and Ostlie along with Eq. 16 (344-346). ρ is the local density, X the mass fraction of hydrogen, and T_6 is the notation for temperature $T \times 10^{-6}$.

While stars are burning only hydrogen, they are considered to be in the main sequence stage. Once they start burning helium they begin the post-main sequence part of their lives. New chains are introduced including the 3α chain, which fuses helium to produce carbon. In this paper we are only concerned with the star's structure during the main sequence and will not take these other chains into account, but acknowledge that they do exist.

When a star forms from a planetary cloud with carbon, nitrogen, and oxygen, another cycle can occur during the main sequence, known as the CNO cycle. Like the latter of the p-p chains, the CNO cycle relies on atoms other than hydrogen to fuse, fission, and produce atomic helium. The equation for the total energy generation from the CNO cycle is

$$\varepsilon_{CNO} = 8.67 \times 10^{23} \rho X X_{CNO} T_6^{-2/3} e^{-152.28 T_6^{-1/3}} \quad \text{Eq. 16}$$

where X_{CNO} is the total fractional abundance of carbon, nitrogen, and oxygen present. With typical compositions, energy generated from the p-p chain is significant enough for the CNO chain to be considered negligible, although, with higher mass stars, the interior pressure is great enough for the CNO cycle to have an impact.

Determining how energy is transported through the star, as measured by temperature changes, is the next step in constructing the stellar interior. The three thermodynamic methods of energy transport are radiation, convection, and conduction.

Like the CNO in energy generation, energy transportation from conduction is negligible in stars. Contributions from radiation and convection need to be considered separately.

Radiation transport relies on electromagnetic radiation (photons) to carry energy out towards the surface. Fully understanding the derivation for the radiation temperature gradient (change in temperature due to radiation) requires going back and explaining the radiation pressure gradient and flux. For the sake of getting straight to the point, the radiation temperature gradient is given as

$$\frac{dT}{dr} = -\frac{3}{16\sigma} \frac{\bar{\kappa}\rho}{T^3} \frac{L_r}{4\pi r^2}, \quad \text{Eq. 17}$$

where σ is the Stefan-Boltzmann constant $5.67 \times 10^{-8} \text{ W}\cdot\text{m}^{-2}\cdot\text{K}^{-4}$ and $\bar{\kappa}$ is the mean opacity. Opacity is defined as the ability for a cross section of substance to absorb photons per mass, measured in $\text{m}^2\cdot\text{kg}^{-1}$ (Carroll 265). The amount of energy radiating through a star is dependent on opacity because as opacity increases, more photons will be absorbed and not continue the journey.

Four different opacities are summed up to generate the mean opacity. The first is bound-bound opacity and is caused when an electron still bound to an atom absorbs the photon energy and changes to a higher energy level (Carroll 269). In a stellar interior, the energy received by an electron is so great that it will always be enough to ionize any atom with a bound electron. Bound-bound opacity is the only negligible contributor and is not taken into account when calculating opacity.

Unlike bound-bound, the ionization of atoms, known as bound-free absorption, is important when calculating the mean opacity. The bound-free absorption opacity is calculated as such:

$$\kappa_{bf} = 4.34 \times 10^{24} \frac{1}{t} Z(1+X) \frac{\rho}{T^{3.5}}, \quad \text{Eq. 18}$$

where Z is the mass fraction of metals (all elements other than hydrogen and helium). The term t is known as the guillotine factor and is used to turn down the bound-free opacity contribution when the surrounding temperature is great enough to ionize hydrogen (158,140 K). When using t , we will have its value go from 1 to 100 when the temperature is greater than 158,140 K.

The third contributor to the mean opacity is free-free absorption. It occurs when electrons already free from atoms absorb photons and use them to gain kinetic energy. The equation for calculating free-free absorption opacity is

$$\kappa_{ff} = 3.68 \times 10^{21} (1-Z)(1+X) \frac{\rho}{T^{3.5}}. \quad \text{Eq. 19}$$

The last contributor to mean opacity is the scattering of photons by free electrons. Electron scattering opacity is simple because it is only dependent on composition:

$$\kappa_{es} = .02(1+X). \quad \text{Eq. 20}$$

The sum of all these opacity contributors gives us the mean opacity,

$$\bar{\kappa} = \kappa_{bb} + \kappa_{bf} + \kappa_{ff} + \kappa_{es}, \quad \text{Eq. 21}$$

where $\kappa_{bb} \approx 0$.

The other type of significant energy transport is adiabatic convection, or the thermal interactions of moving gas or fluid. The temperature gradient for adiabatic convection is

$$\frac{dT}{dr_{ad}} = -\left(1 - \frac{1}{\gamma}\right) \frac{\mu m_H}{k} \frac{GM_r}{r^2}, \quad \text{Eq. 22}$$

where γ is a specific heat parameter ($\gamma = \frac{5}{3}$ for atomic hydrogen and helium) μm_H is the mass of atomic hydrogen (1.67×10^{-27} kg), and k is Boltzmann's constant 1.38×10^{-23} J·K⁻¹. Whichever temperature gradient (Eq. 17 or Eq. 22) is shallower becomes the dominating energy transport. In other words, Eq. 17 is used when its calculated value, from local conditions, is greater than that of adiabatic convection, and vice versa.

The equation of state will also be important when modeling stellar interiors. It combines the pressure calculated by the ideal gas law and light pressure due to photon momentum:

$$P = \frac{\rho k T}{\mu m_H} + \frac{4\sigma T^4}{3c}, \quad \text{Eq. 23}$$

where c is the speed of light 3.00×10^8 m·s⁻¹. The ideal gas law can be used because a gas acts ideally when molecules don't tend to "stick" to each other. Star temperatures are large enough to keep the gas molecules separate from each other. The consideration of light pressure is due to the total number of photons carrying enough momentum to affect the pressure. Eq. 23 gives us another way to relate temperature, pressure, and density. Density in particular is important for relating to local conditions such as P and T . It shows that density also changes with respect to r . For basic models, making assumptions about density will prove useful in simplifying the modeling process.

ASSUMPTIONS FOR A SIMPLE MODEL: DENSITY AS A CONSTANT

The equations of stellar structure cannot be solved analytically. To do so would require using separation of variables to integrate both sides. Only relatively simple

differential equations can have an analytical solution. Linear and low order nonlinear equations usually have solutions, but the equations of stellar structure are fourth order and nonlinear. In cases such as this, a solution is estimated through numerical methods. We can begin with simple models based on assuming how one or more characteristics might behave within a star. If we take density and assume it's not a function of radius, but instead constant throughout the star, then the equations will simplify to something we can solve analytically for an initial basic model.

Before getting started, we need to assign boundary conditions for when $r = 0$ and $r = R_*$. Carroll and Ostlie give the set of known boundary conditions and state that they are used as the limits and initial conditions when finding a numerical solution (367):

$$\left. \begin{array}{l} M_r \rightarrow 0 \\ L_r \rightarrow 0 \end{array} \right\} \text{ as } r \rightarrow 0 \quad \text{Eq. 24}$$

$$\left. \begin{array}{l} T \rightarrow 0 \\ P \rightarrow 0 \\ \rho \rightarrow 0 \end{array} \right\} \text{ as } r \rightarrow R_* \quad \text{Eq. 25}$$

The **Eq. 24** boundary conditions are easily understandable, since the center contains no mass and the outward luminosity cannot travel through it. The boundary conditions in **Eq. 25** aren't true for a real star and create problems for numerical solutions (see in later discussion). Also, we ignore the third boundary condition in **Eq. 25** for our constant density assumption because it creates a discontinuity in the density function at $r = R_*$. Fortunately, the other boundary conditions are useful when finding analytical solutions after making our assumptions on density. The boundary conditions will help find the value of constants that result from solving an indefinite integral.

Beginning with the mass conservation equation, assigning ρ as a constant makes **Eq. 8** a single-variable problem. Separating variables and integrating, as in **Eq. 9**, gives us an easy analytical solution for mass conservation:

$$M_r = \frac{4}{3} \pi r^3 \rho + M_0. \quad \text{Eq. 26}$$

Using our mass boundary condition, we can eliminate M_0 :

$$M_r = \frac{4}{3} \pi r^3 \rho. \quad \text{Eq. 27}$$

Substituting **Eq. 27** into the hydrostatic equilibrium equation **Eq. 6** also gives us a single-variable problem that has an analytical solution. By again using separation of variables, we get

$$P_r = -\frac{2}{3} G \rho^2 \pi r^2 + P_0. \quad \text{Eq. 28}$$

The pressure boundary condition says $P_{R_*} = 0$, so then

$$0 = -\frac{2}{3} G \rho^2 \pi R_*^2 + P_0$$

$$P_0 = \frac{2}{3} G \rho^2 \pi R_*^2 \quad \text{Eq. 29}$$

$$P_r = -\frac{2}{3} G \rho^2 \pi r^2 + \frac{2}{3} G \rho^2 \pi R_*^2$$

$$= -\frac{2}{3} G \rho^2 \pi (r^2 - R_*^2). \quad \text{Eq. 30}$$

For energy generation and the temperature gradient, we follow a different approach suggested by Prof. Dan Watson of the University of Rochester. Instead of dealing with the radiative or convective energy transport equations, we'll use the ideal gas law,

$$T_r = \frac{P_r \mu m_H}{\rho k} \quad \text{Eq. 31}$$

and substitute in **Eq. 30** to get an analytic solution for temperature (Watson 14). After simplifying, we get

$$T_r = -\frac{2G\rho\pi r^2 \mu m_H}{3k} + \frac{2G\rho\pi R_*^2 \mu m_H}{3k}. \quad \text{Eq. 32}$$

Note that the second term is the constant T_0 . Also, evaluating **Eq. 32** at R_* agrees with the boundary condition of zero.

The only analytical solution left to find is L_r . The best way to determine an equation for L_r isn't through **Eq. 12**. Instead, we can isolate it in the only other place it appears, **Eq. 17**. Differentiating **Eq. 32** gives us a third equation for $\frac{dT}{dr}$,

$$\frac{dT}{dr} = -\frac{4G\rho\pi r \mu m_H}{3k}, \quad \text{Eq. 33}$$

which we substitute into **Eq. 17**. Assuming only free-free opacity we also substitute in **Eq. 19** and solve for L_r to obtain

$$L_r = \frac{256}{9} \frac{G\pi^2 r^3 \sigma T^{6.5} \mu m_H}{\rho (3.68 \times 10^{21}) (1-Z)(1+X)}. \quad \text{Eq. 34}$$

Since L_r is the luminosity generated within r , it should approach L_* as $r \rightarrow R_*$.

However, with temperature going to zero at the same time, **Eq. 34** also becomes zero. To

get around this, Watson points out that the total luminosity is generated within $\frac{R_*}{2}$

(Watson 15). This fact will be evident when we use temperature, density, and

composition to graph the energy generated ϵ . We can now use **Eqs. 27, 31, 32, 34**, and

15 to plot out the interior mass, pressure, temperature, determine the total luminosity, and plot the energy generation (in that order).

Before building our model, we need to decide on a stellar composition. We'll use the standard mass fractions for metal-rich Population I stars for X and Z , which are 0.7 and 0.03, respectively. The older Population II stars have a lower metal composition. These correspond to a zero age main sequence (ZAMS) star just beginning its hydrogen-burning process. We're modeling ZAMS stars because no additional helium has yet been added to the system.

The observational data available to use are surface temperature, total luminosity, and radius, and mass. Temperature and luminosity are actually used to determine the radius, while the mass is determined from its movements relative to nearby stars (usually in a multi-star system). Radius and mass are the most important because we need them to make our density assumption by taking the total mass over the equated spherical volume from the known radius.

For our model, we're selecting stars based on their surface temperature, or spectral type. Spectral types are classified by one of seven letters, beginning with M as the coolest and up through K, G, F, A, B, and O, which is the hottest spectral type. Each letter is then followed by a number 0-9, where 0 is the hottest and 9 is the coldest. For example, the spectral type of our sun is designated G2. A star of spectral type G1 would be hotter. We can determine the spectral types by their color. Cool stars in the range of M and K are red or orange. With increasing temperature, the color changes to yellow, white, and then blue for the hottest stars.

The spectral types we selected are listed in **Table 1**, along with the observed mass and radius taken from Carroll and Ostlie (A13-14). The mass and radii were used to compute the average density and placed in the last column. We also used **Eq. 29**, T_0 from **Eq. 32**, and **Eq. 34** evaluated at $\frac{R_*}{2}$ to calculate the core pressure, temperature and total luminosity for each spectral type (**Table 2**). The columns in **Tables 1** and **2** for ρ , P_0 , T_0 , and L_{tot} were plotted against the radius of each spectral type (**Figure A1a-d**). Core conditions and total luminosity for the various stellar masses are plotted in **Figure A1a-d**.

The core densities in **Figure A1a** are also the star's average density due to our assumption of constant density throughout the star. Despite the increasing stellar mass, the core density is decreasing. It's a direct consequence of the stellar volume increasing at a much greater rate when moving up the spectrum to stars with more mass. Comparing an A0 and B5 star, the B5 has approximately twice the mass of an A0 star. It also has about 1.5 times the radius. Because $V \propto R^3$, the volume of the B5 star is 3.5 times as large. The decreasing core density may be the cause for a decreasing core pressure in more massive stars, as seen in **Figure A1b**. Hydrostatic equilibrium should cause the core pressure to increase if it's going to support more mass.

Core temperature (**Figure A1c**) increases with more massive stars, as expected for generating a higher pressure. However, the rate of core temperature increase with respect to stellar mass does not compare to the rate of decrease for core density. Note that core pressure from M5 to O5 varies by about 4×10^7 K, while core pressure is changing rapidly enough to be plotted on a logarithmic scale. The ideal gas equation says $P \propto T\rho$.

The actual core density change with increasing stellar mass must have a more positive gradient than in this model.

Using our core conditions in conjunction with **Eq. 30** and **32**, we see how pressure and temperature are structured between the core and surface. **Figure A2a-c** has the interior pressure and temperature plotted for each of our spectral types, along with the interior energy generation to show where most of the stellar luminosity is being produced. Pressure and temperature appear to change more rapidly as they approach zero at the surface, though we'd expect more of an asymptotical approach. In **Figure A2c** a large portion of the energy is being generated within $.5R_*$, but a significant amount is being generated beyond that distance. Also, the cooler red and orange stars are generating more energy per kg's near the core than the hot blue stars, with the exception of the O5 star. This is a result of the pressure and density flaw in our model.

To decide how well our model compares with observational data, we'll use the total luminosity and surface temperature[†]. Temperature and luminosity are the easiest data to obtain. The two are plotted L vs. T in something known as the Hertzsprung-Russell (H-R) diagram. It relates the two properties and distinguishes different types of stars. **Figure A3** is a typical H-R diagram. The absolute magnitude scale in **Figure A3**, like luminosity, tells how bright a star is, but when placed at a set distance of 10 pc (32.57 ly). Stars that fall on or near the path going from the cool dim corner (low stellar mass) to the hot bright corner (high stellar mass) are considered main sequence. The hot dim stars are white dwarf. They are what remain after a relatively low-mass star sheds its

[†] Since our assumption that $T \rightarrow 0$ at the surface, we'll use the observed surface temperature for each spectral type.

outer layers near the end of its life. The cool bright stars are known as the giants. Stars move off the main sequence and become giants when they begin fusing helium.

With total luminosity and surface temperature data taken from the same location of Carroll and Ostlie as in **Table A1**, we superimpose our L_{tot} from **Table A2** and observed surface temperatures from **Table A3** to get the **Figure A4** H-R diagram (A13-14). The calculated luminosity follows the observational data very closely. The theoretical luminosity falls below the observational data for low-mass stars, but deviates above it for stars of greater mass.

This model is very promising, what still needs some work. It handles luminosity very well, as demonstrated with the H-R diagram, but has a few flaws. Its greatest problem is the core density, which leads to problems with pressure. Already, we can determine that more massive stars contain a higher mass fraction near their core than do low-mass stars. Changing our assumption with density will help build more accurate stellar models.

ASSUMPTIONS FOR A SIMPLE MODEL: LINEAR DENSITY

The even distribution of mass is not very realistic. More likely, density would be greater at the center. Watson uses the assumption that density increases linearly with respect to radius, which he calls the linear stellar model:

$$\rho_r = \rho_0 \left(1 - \frac{r}{R_*} \right). \quad \text{Eq. 35}$$

For purposes of simplicity, we will use x for $\frac{r}{R_*}$ such that

$$\rho_r = \rho_0(1-x). \quad \text{Eq. 36}$$

In this section we will use **Eq. 36** as our new density assumption and use similar methods from the previous section to build a second model we can compare to our first.

Despite density no longer being a constant, we can still solve the stellar structure equations analytically. After substituting **Eq. 36** into **Eq. 8** and separating the variables we have

$$dM_r = 4\pi r^2 \rho_0(1-x)dr. \quad \text{Eq. 37}$$

Using $x = \frac{r}{R_*}$, we can substitute in $R_*^2 x^2$ to eliminate r^2 :

$$dM_r = 4\pi R_*^2 x^2 \rho_0(1-x)dr. \quad \text{Eq. 38}$$

We substituted in x to simplify things, but we also need to be able to integrate with respect to x . Differentiating x with respect to r gives the equation

$$\frac{dx}{dr} = \frac{1}{R_*}, \quad \text{Eq. 39}$$

which can be rearranged to form

$$dr = R_* dx. \quad \text{Eq. 40}$$

Eq. 40 substitutes into **Eq. 38** to eliminate r completely and enable it to be integrated with respect to x :

$$dM_r = 4\pi R_*^3 x^2 \rho_0(1-x)dx. \quad \text{Eq. 41}$$

After integrating, we get our analytical solution for mass conservation,

$$M_r = 4\pi R_*^3 \rho_0 \left(\frac{1}{3} x^3 - \frac{1}{4} x^4 \right), \quad \text{Eq. 42}$$

and by taking into account our boundary conditions, we get the formula for core density,

$$\rho_0 = \frac{M_*}{4\pi R_*^3 \left(\frac{1}{3} - \frac{1}{4} \right)}. \quad \text{Eq. 43}$$

Compared to our analytical solution for mass conservation from the previous section, the only changes are replacing r^3 with R^3 and including a factor of $\left(\frac{1}{3}x^3 - \frac{1}{4}x^4 \right)$.

For the remaining equations the process used in obtaining analytical solutions is still the same as when we assumed constant density. Through the same substitutions and integrations we end up with the following analytical solutions for pressure, temperature, and luminosity:

$$P_r = \frac{1}{36} G\pi R_*^2 \rho_0^2 (-9x^4 + 28x^3 - 24x^2) + P_0 \quad \text{Eq. 44}$$

$$P_0 = -\frac{1}{36} G\pi R_*^2 \rho_0^2 (-9 + 28 - 24) \quad \text{Eq. 45}$$

$$T_r = \frac{1}{36k} G\pi R_*^2 \rho_0 \mu m_H (1-x) (-9x^2 + 10x + 5) \quad \text{Eq. 46}$$

$$T_0 = \frac{5}{36k} G\pi R_*^2 \rho_0 \mu m_H \quad \text{Eq. 47}$$

$$L_r = -\frac{16}{27k} \frac{G\pi^2 R_*^3 x^2 \sigma T^{6.5} \mu m_H (27x^2 - 38x + 5)}{\rho_0 (1-x)^2 (3.68 \times 10^{21}) (1-Z)(1+X)} \quad \text{Eq. 48}$$

$$L_{R_*/2} = \frac{116}{27k} \frac{G\pi^2 R_*^3 \sigma T^{6.5} \mu m_H}{\rho_0 (3.68 \times 10^{21}) (1-Z)(1+X)}. \quad \text{Eq. 49}$$

The calculated core density, pressure, temperature, and total luminosity for each spectral type are listed in **Table B1**. As with the constant density model, the core conditions and interior structure were graphed (**Figure B1a-d** and **Figure B2a-c**, respectively), and another H-R diagram was constructed (**Figure B3**).

Our new density assumption did very little to fix the pressure issue experience in the previous section. The values in **Figures B1a-b** have only increased from our previous model by a factor of 4 and 3.33, respectively (these differences appear as a vertical shift on the logarithmic scale). If the density structure is the same in every star, this pattern will probably continue. Density in high-mass stars must change more rapidly near the center. Also, the core temperature was decreased by a factor of 0.83. Total luminosity is the only parameter affected positively. The luminosity was decreased significantly, creating an unexpected problem with our H-R diagram for the linear density model.

For the interior structures (**Figure B2a-c**) pressure and temperature do not drop down sharply like in our previous model, but behave asymptotically (more with pressure than temperature). Energy generation in **Figure B2c** is pushed more towards the stars' centers. Since our calculations for total luminosity are dependent on all the energy generation occurring within $0.5R_*$, this model more accurately determines a star's energy output.

The problem with our new interior temperature and energy generation model is the fact that the maximum for both is not at the core. Interior temperature peaks at about $0.15R_*$ and energy generation peaks at about $0.1R_*$. The assumption of linear density caused a higher-degree polynomial to be generated after each integration that obtained analytical solutions for mass, pressure, and temperature. The peaks between the core and surface are a consequence of this radius-dependent polynomial resulting from our linear assumption.

The less accurate luminosity value is shown in the updated H-R diagram (**Figure B3**). All calculated values are now less than the observational data. However, the calculated luminosity is now comparable with the observational data. The data for low-mass stars actually come very close to the observable data, but diverge with more massive stars.

This model is a slight improvement of our previous one, but it still has some of the same flaws, along with new ones. The interior structure is closer to what we'd expect. However, the calculated total luminosity is now much lower than the observational data, though the shape of its path is still the same. The problems with density and pressure also still exist. These problems can't be completely fixed unless we know exactly how density behaves in stars of every spectral type. It would also be best to know when convective heat transfer dominates over radiative transfer and when the CNO cycle should be considered. The best method for building an accurate stellar model begins with our boundary conditions. We could use them as a starting point for numerical integration to build a model from the outside in without needing to make any assumptions for density. It would model the stellar interior one small step at a time, as opposed to one great leap with our models' analytical solutions.

CONCLUSIONS

Our theoretical models have provided a look into how stars are composed without needing to dig into the interior of every star. Data from both models give similar results on the core conditions and total luminosity of various stellar masses. **Figures A1c** and

B1c both have a linear relationship for high-mass stars and possibly a logarithmic relationship for low- to medium-mass stars, though the linear density model gives high core temperatures. The total luminosity in **Figures A1d** and **B1d** follows a power rule, but the first gives higher luminosity that corresponds better with observational data in **Figure A4**.

For the interior structure, the constant density model has the steepest pressure and temperature change occurring at the stellar surface. The linear density model has it within the interior (about $0.5R_*$ for pressure and $0.8R_*$ for temperature) and behaves asymptotically near the stellar surface. Also, more of the nuclear energy generation in this model occurs within $0.5R_*$, which better agrees with the assumption that the total luminosity comes from within this radius.

Surprisingly, the H-R diagram in the constant density model is much better than our linear density model. The theoretical data overlaps well with the observable data, though they diverge with more massive stars. This may be an indicator of when the CNO cycle needs to be considered. It is also an indicator that a second model is not always better. The linear density model had a more realistic mass distribution, but failed to provide accurate total luminosities.

The optimal model would be to use numerical methods and integrate all stellar structure equations from the surface in towards the core. This is the next step to take in modeling stellar interiors. We would need to choose a step size and set the boundary conditions as our initial conditions. For the analytical models, the surface boundary conditions for density, pressure, and temperature were zero. This, however, will not work for a numerical solution, as it will create situations that divide by zero.

Observable surface conditions, which are easily obtained, would be used instead and could be easily altered with a program such as Microsoft[®] Excel to satisfy the core conditions. This model would also be able to take into account the other conditions, such as the CNO cycle and convective energy transport, which we were unable to use in our analytical models.

These models are only the key to unlocking the rest of the universe. They help test our hypotheses and formulate new ones to better understand the object in question. Even failed models teach us something; the flaws in density and pressure of our analytical models showed that density distribution doesn't work the same in all stars. It is instead more concentrated at the core in more massive stars. That information can then be used to make a better stellar model. Mathematical models may reach a point where they seem flawless, but they can always be improved upon. Technology and numerical methods will always be advancing and providing a better way to understand the universe.

APPENDIX A: CONSTANT DENSITY DATA

Table A1: spectral types modeled

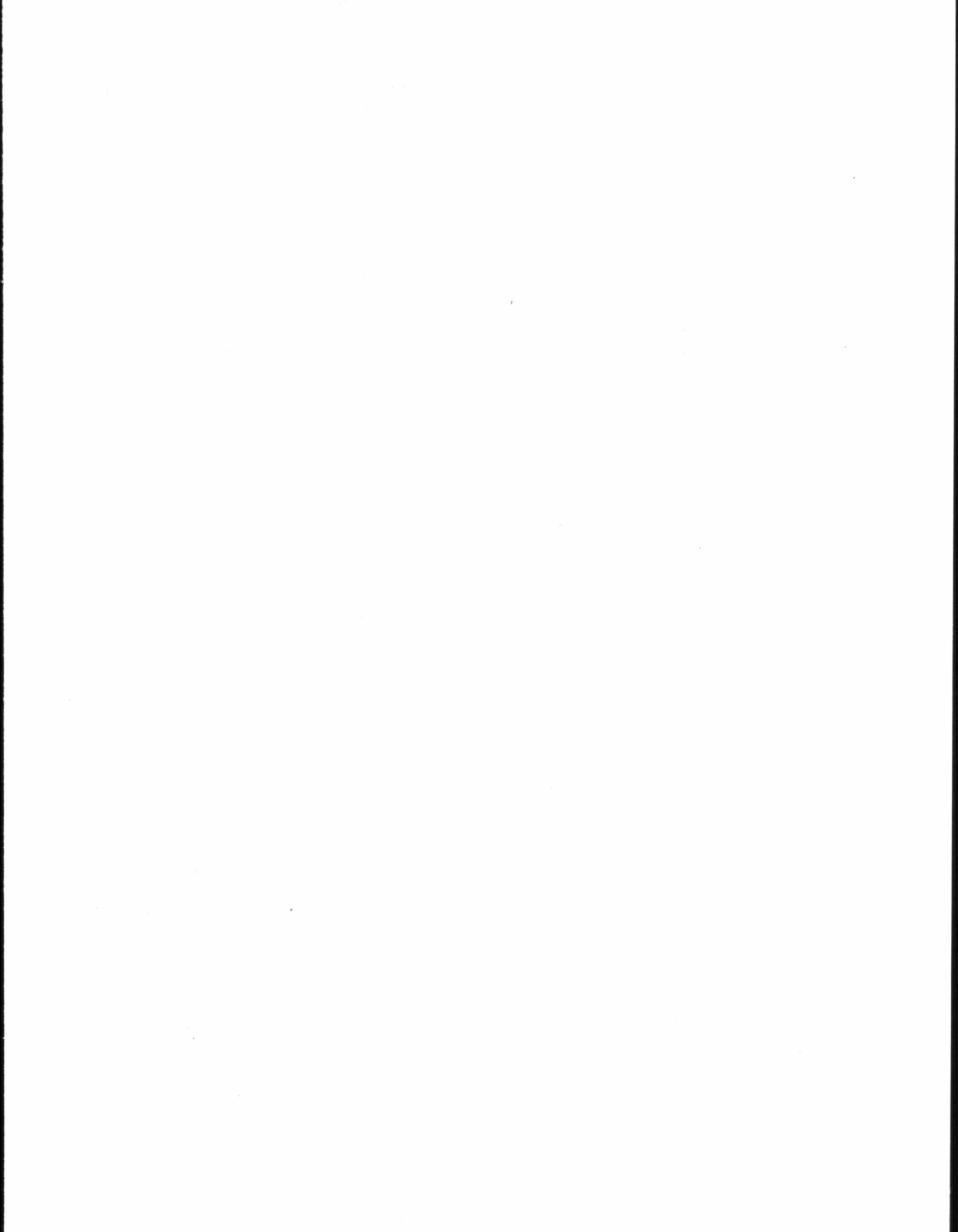
Spectral Type	R/R_{sol}	M/M_{sol}	ρ (kg·m ⁻³)
M5	0.33	0.21	8.23×10^3
M0	0.63	0.51	2.87×10^3
K5	0.68	0.67	3.00×10^3
K0	0.79	0.79	2.26×10^3
G5	0.89	0.92	1.84×10^3
G0	1.10	1.05	1.11×10^3
F5	1.40	1.40	7.19×10^2
F0	1.60	1.60	5.50×10^2
A5	1.90	2.00	4.11×10^2
A0	2.70	2.90	2.08×10^2
B5	4.10	5.90	1.21×10^2
B0	8.40	17.5	4.16×10^1
B5	15.0	60.0	2.51×10^1

Table A2: calculated core conditions

Spectral Type	P_0 (Pa)	T_0 (K)	L_{tot} (W)
M5	5.00×10^{14}	7.36×10^6	2.59×10^{23}
M0	2.22×10^{14}	9.36×10^6	2.47×10^{25}
K5	2.82×10^{14}	1.14×10^7	1.07×10^{26}
K0	2.15×10^{14}	1.16×10^7	2.45×10^{26}
G5	1.81×10^{14}	1.20×10^7	5.33×10^{26}
G0	1.01×10^{14}	1.10×10^7	9.93×10^{26}
F5	6.86×10^{13}	1.16×10^7	4.28×10^{27}
F0	5.25×10^{13}	1.16×10^7	8.35×10^{27}
A5	4.13×10^{13}	1.22×10^7	2.61×10^{28}
A0	2.13×10^{13}	1.24×10^7	1.69×10^{29}
B5	1.66×10^{13}	1.66×10^7	5.83×10^{30}
B0	8.27×10^{12}	2.41×10^7	1.89×10^{33}
O5	9.56×10^{12}	4.63×10^7	1.24×10^{36}

Table A3: observational data

Spectral Type	T_{*} (K)	L_{tot} (W)
M5	3240	4.29×10^{24}
M0	3850	3.00×10^{25}
K5	4350	5.85×10^{25}
K0	5250	1.64×10^{26}
G5	5780	3.90×10^{26}
G0	6030	5.85×10^{26}
F5	6440	1.13×10^{27}
F0	7200	2.54×10^{27}
A5	8200	5.46×10^{27}
A0	9520	2.11×10^{28}
B5	15400	3.24×10^{29}
B0	30000	2.03×10^{31}
O5	44500	3.08×10^{32}



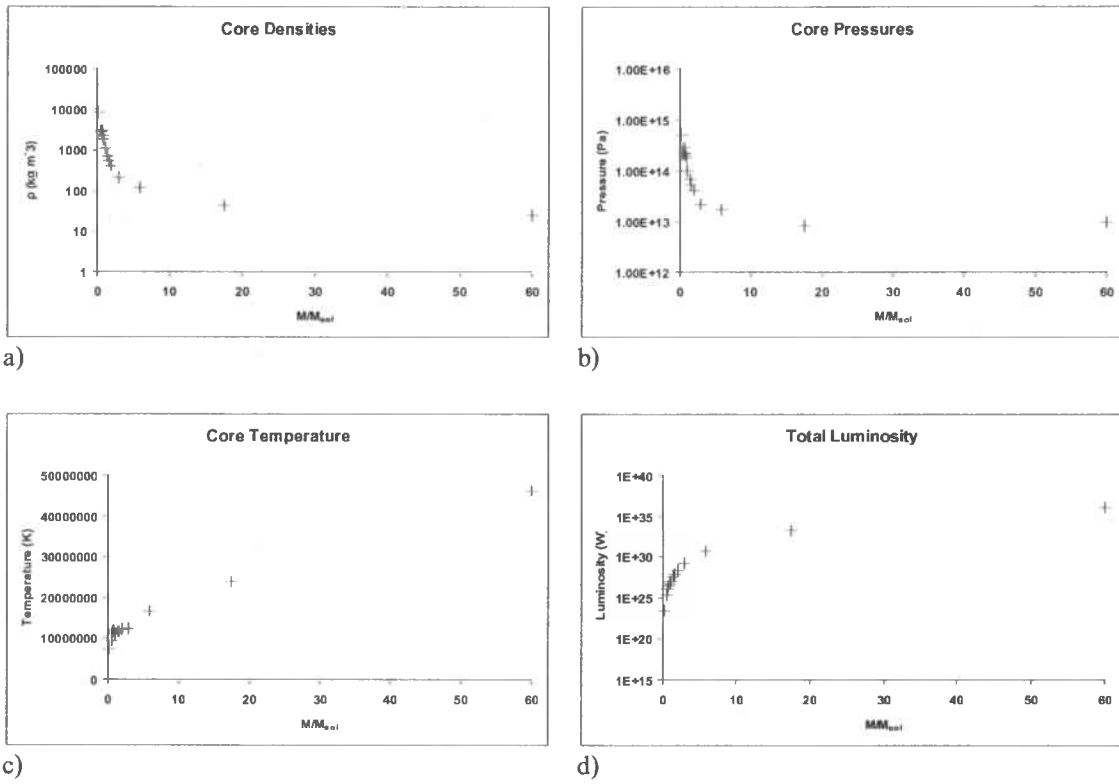
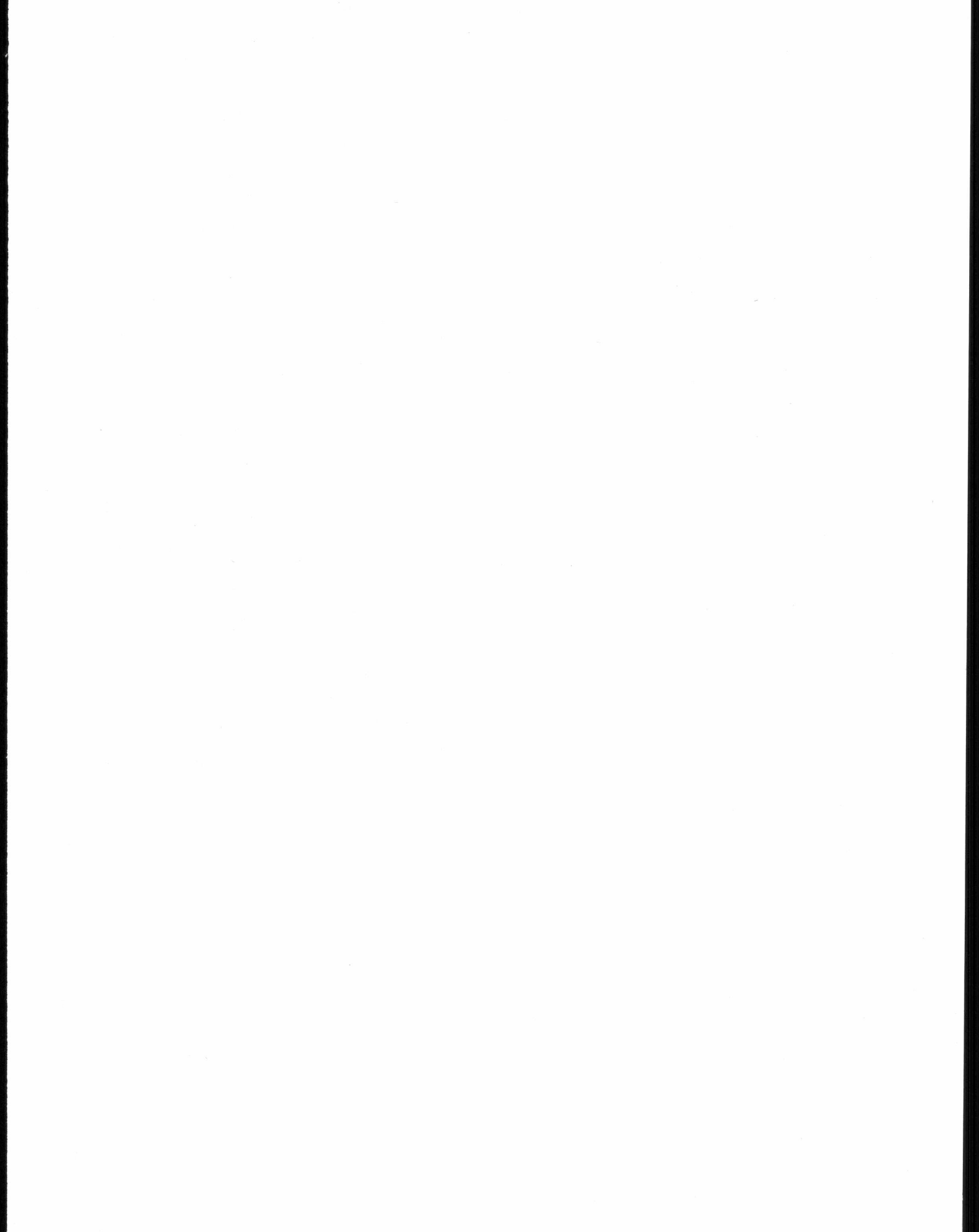
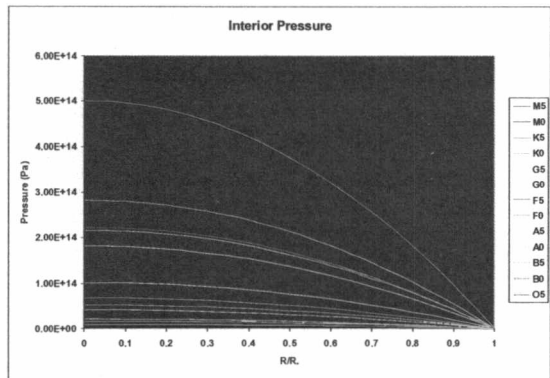
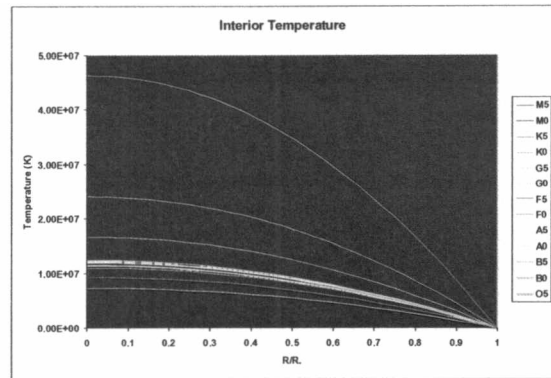


Figure A1: a) core densities, b) pressures, c) temperatures, and d) total luminosities for each of the various main sequence spectral types.

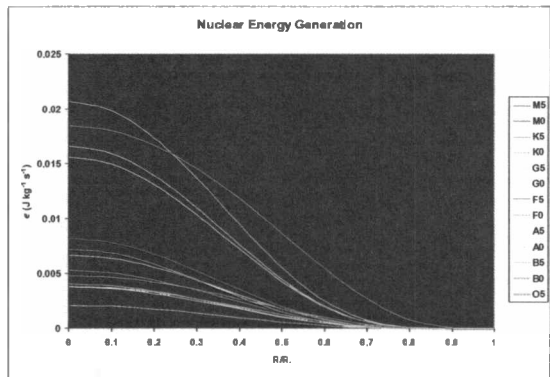




a)

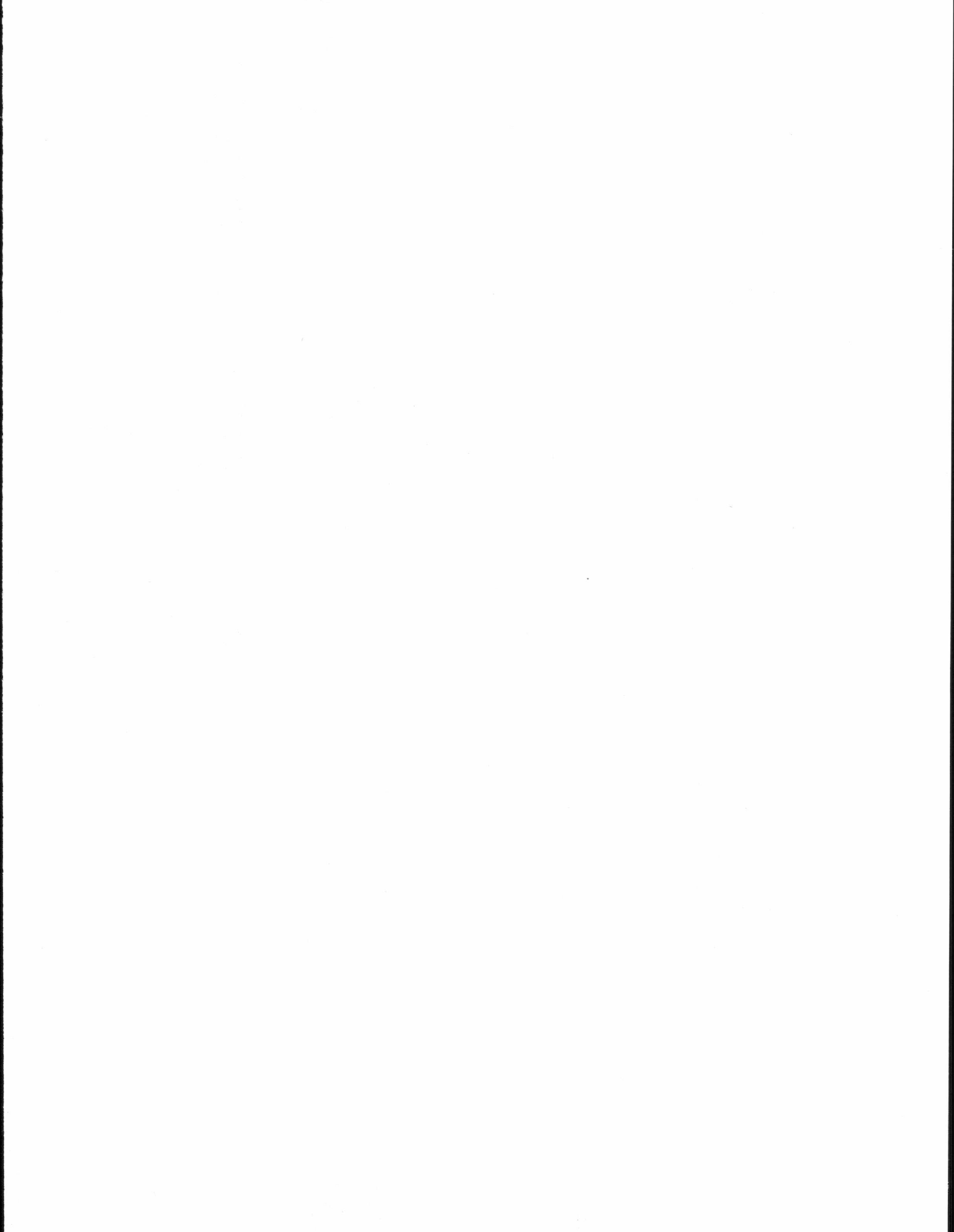


b)



c)

Figure A2: stellar interior structure for the constant density model.



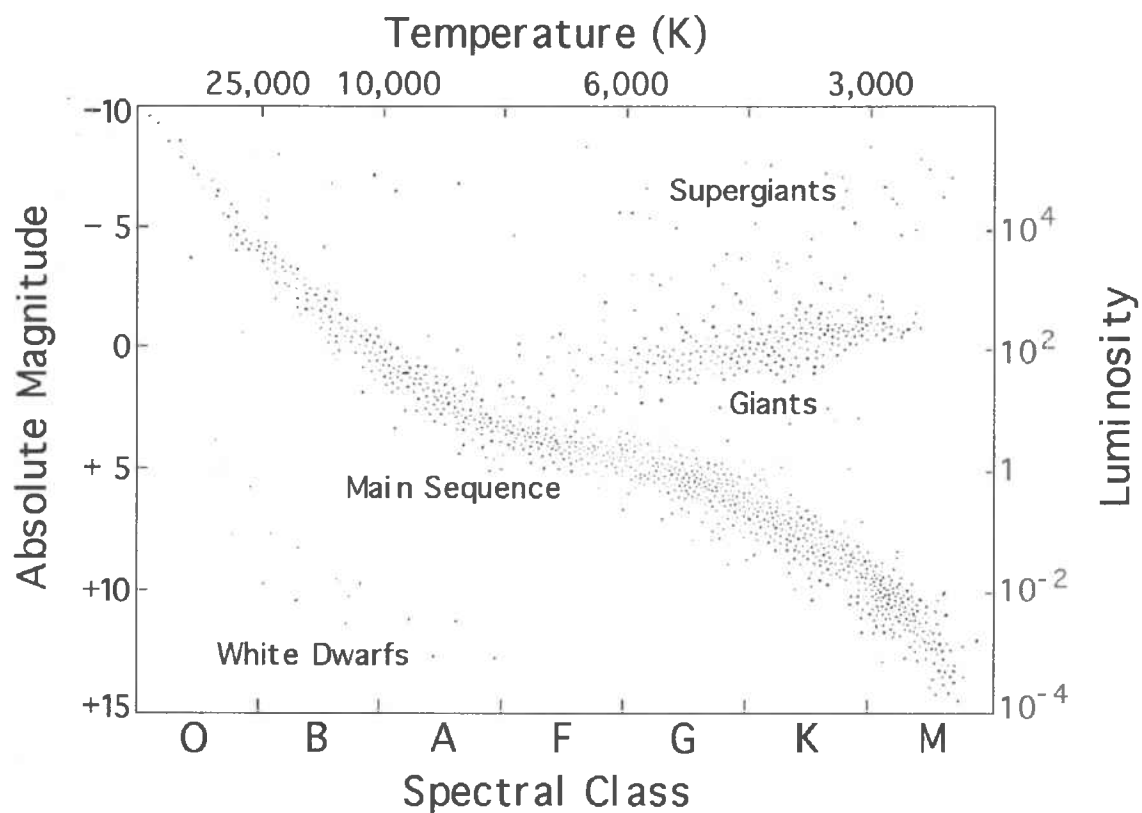
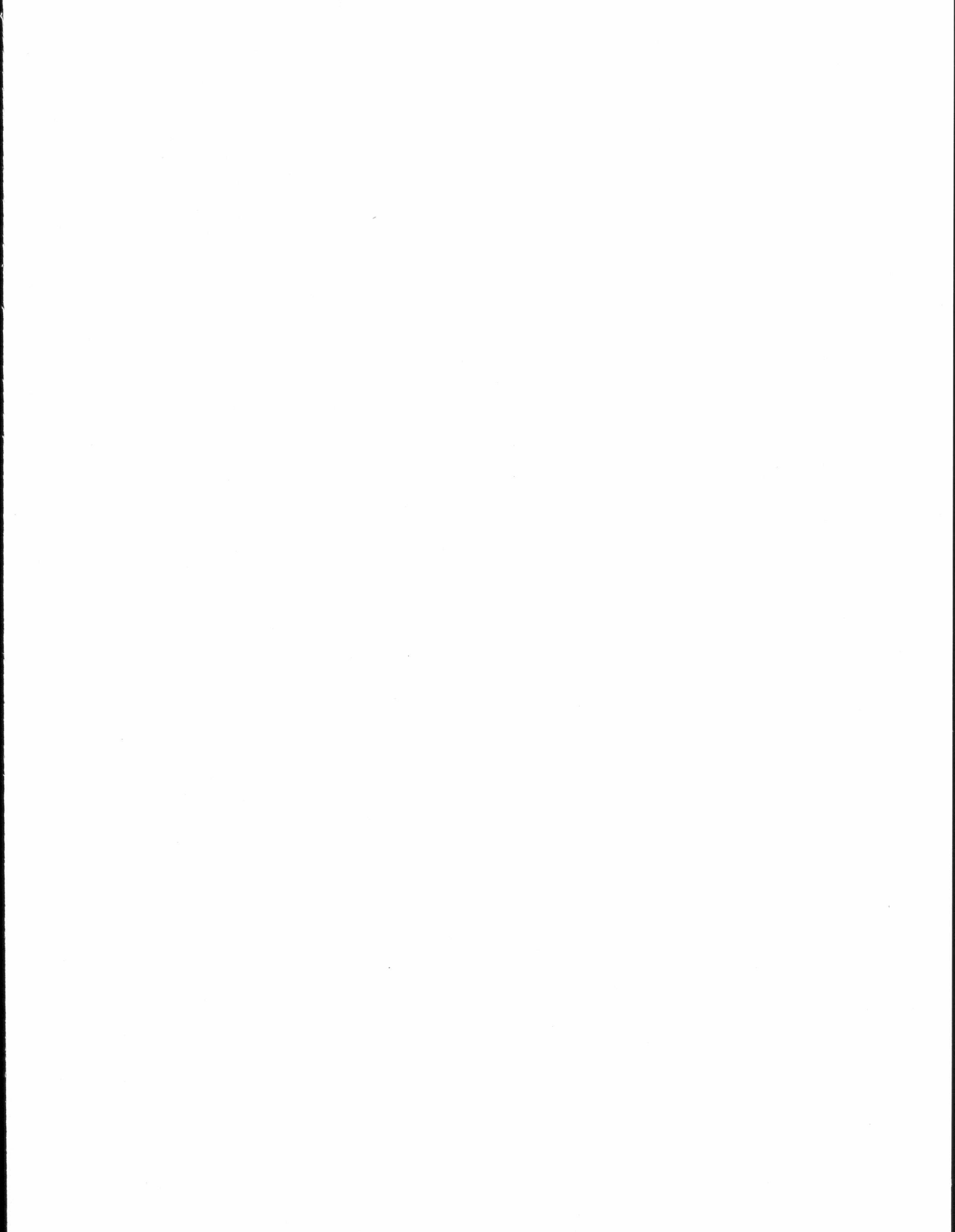


Figure A3: a typical H-R diagram.

Barbier, Louis, and Beth Jacob. "Ask Us - Stars." *NASA's Cosmicopia*. 20 Dec. 2006. NASA. 9 Mar. 2007
 <<http://imagine.gsfc.nasa.gov/docs/teachers/lifecycles/Image31.gif>>.



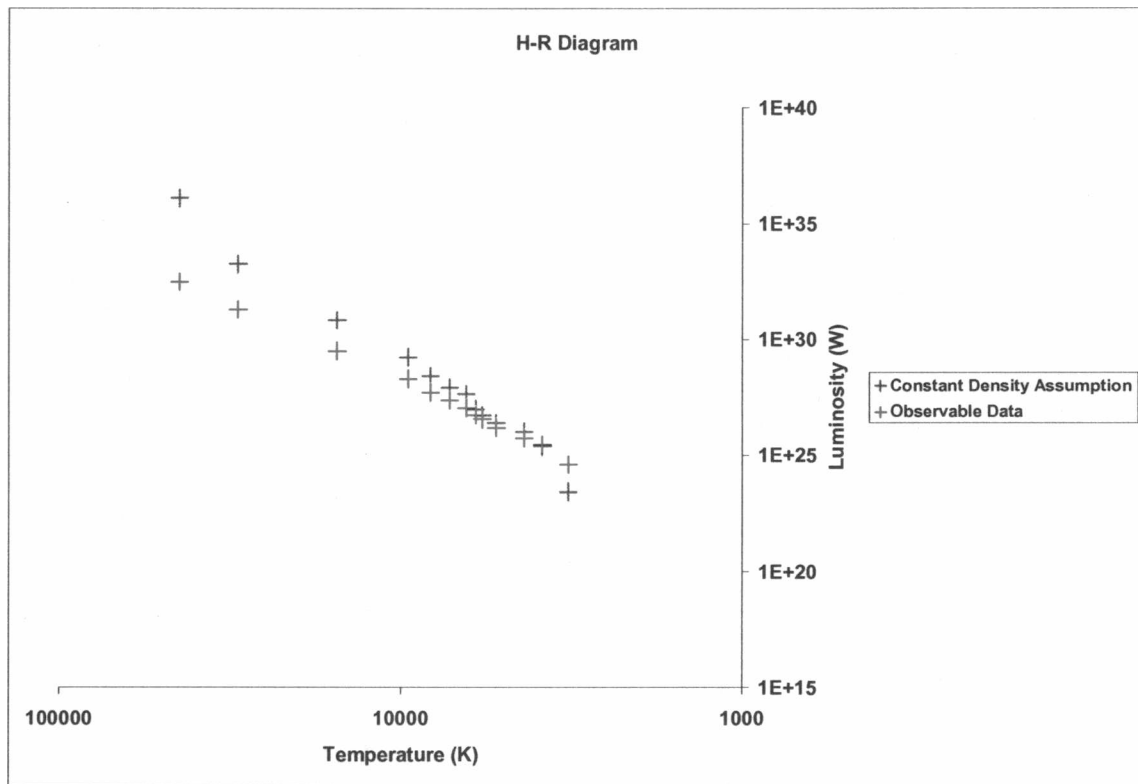
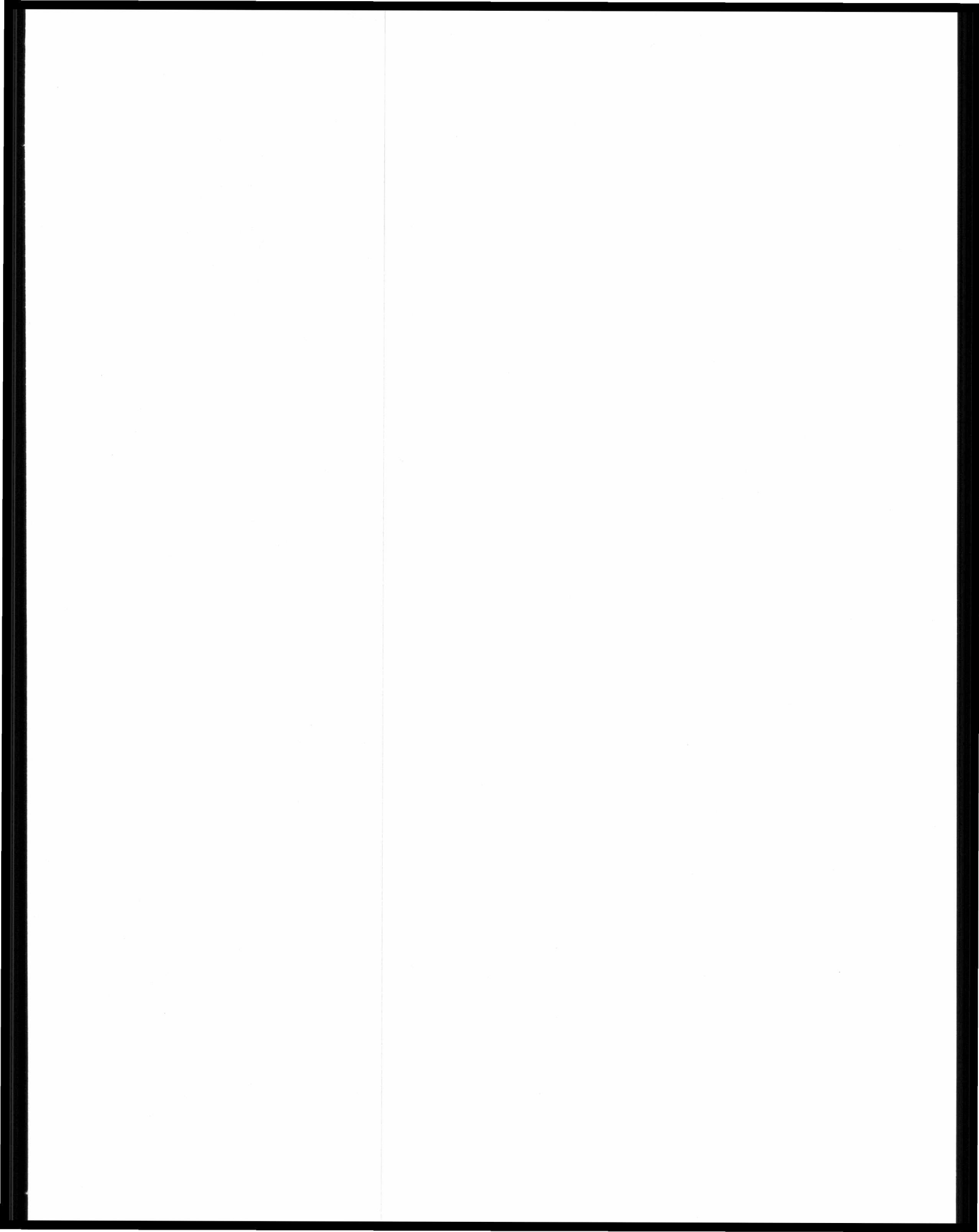


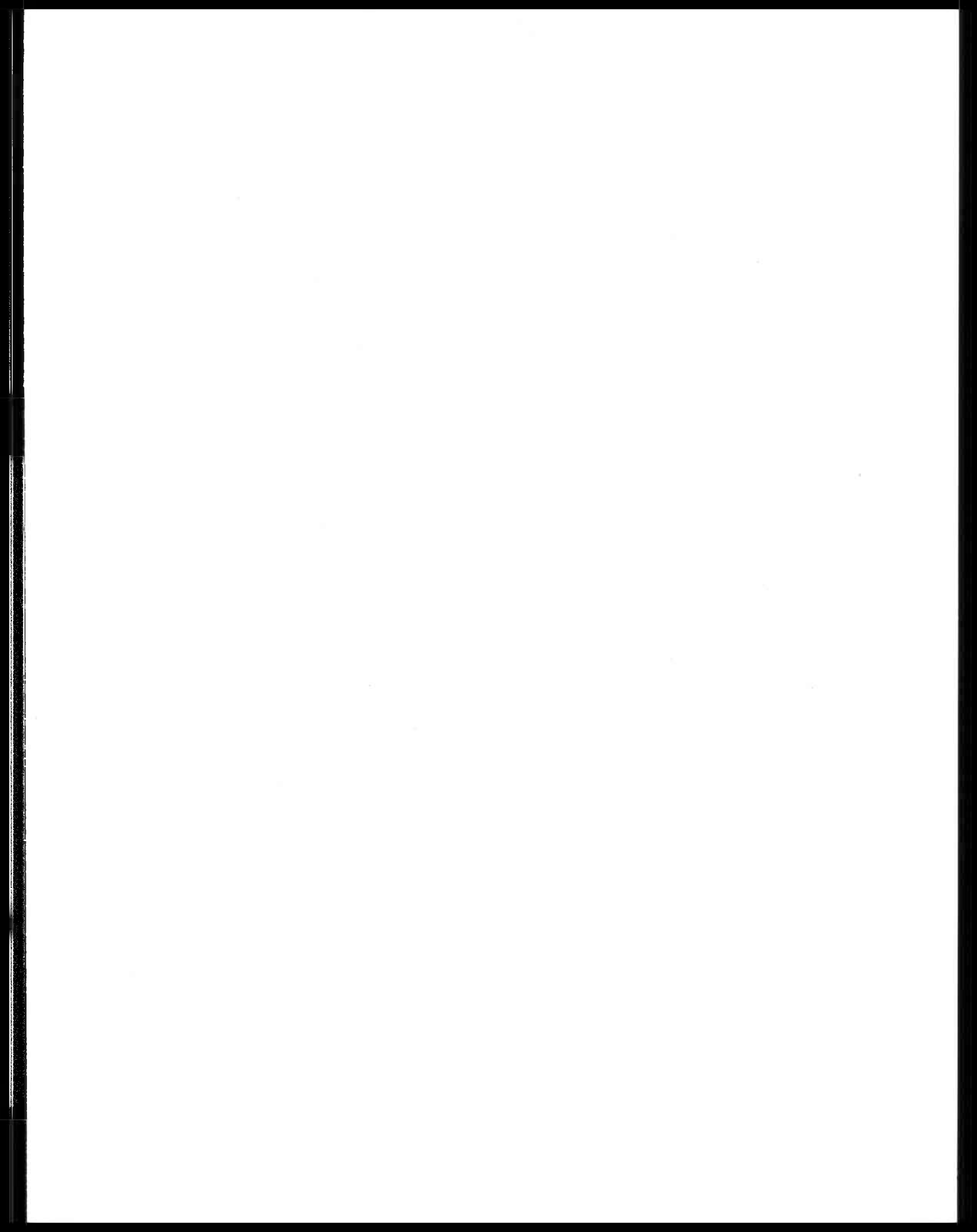
Figure A4: an H-R diagram comparing data from the constant density theoretical model with observable data.

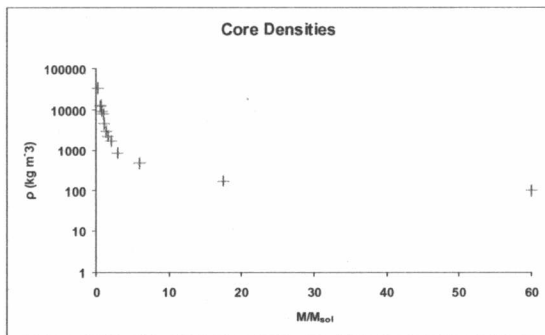


APPENDIX B: LINEAR DENSITY DATA

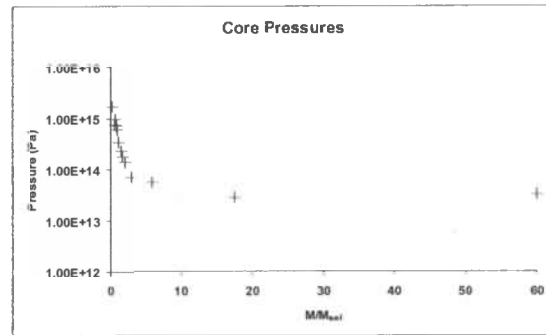
Table B1: calculated core conditions for the linear density model

Spectral Type	ρ_0 (kg·m ⁻¹)	P_0 (N·m ⁻²)	T_0 (K)	L_{tot} (J·s ⁻¹)
M5	3.29×10^4	1.67×10^{15}	6.13×10^6	4.52×10^{17}
M0	1.15×10^4	7.40×10^{14}	7.80×10^6	4.31×10^{19}
K5	1.20×10^4	9.41×10^{14}	9.50×10^6	1.86×10^{20}
K0	9.03×10^3	7.18×10^{14}	9.64×10^6	2.47×10^{20}
G5	7.36×10^3	6.04×10^{14}	9.96×10^6	9.30×10^{20}
G0	4.45×10^3	3.37×10^{14}	9.20×10^6	1.73×10^{21}
F5	2.88×10^3	2.29×10^{14}	9.64×10^6	7.47×10^{21}
F0	2.20×10^3	1.75×10^{14}	9.64×10^6	1.46×10^{22}
A5	1.64×10^3	1.38×10^{14}	1.01×10^7	4.56×10^{22}
A0	8.30×10^2	7.09×10^{13}	1.04×10^7	2.95×10^{23}
B5	4.82×10^2	5.52×10^{13}	1.39×10^7	1.19×10^{25}
B0	1.66×10^2	2.76×10^{13}	2.01×10^7	3.29×10^{27}
O5	1.00×10^2	3.19×10^{13}	3.86×10^7	2.16×10^{30}

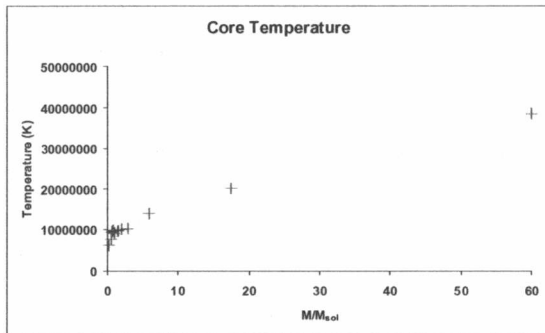




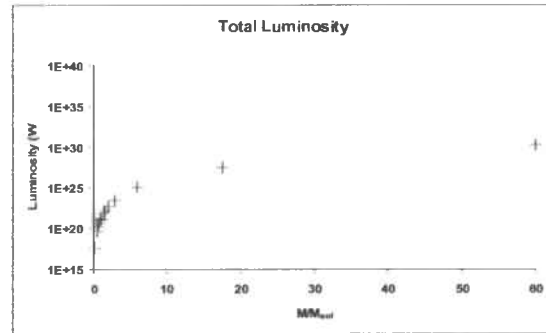
a)



b)

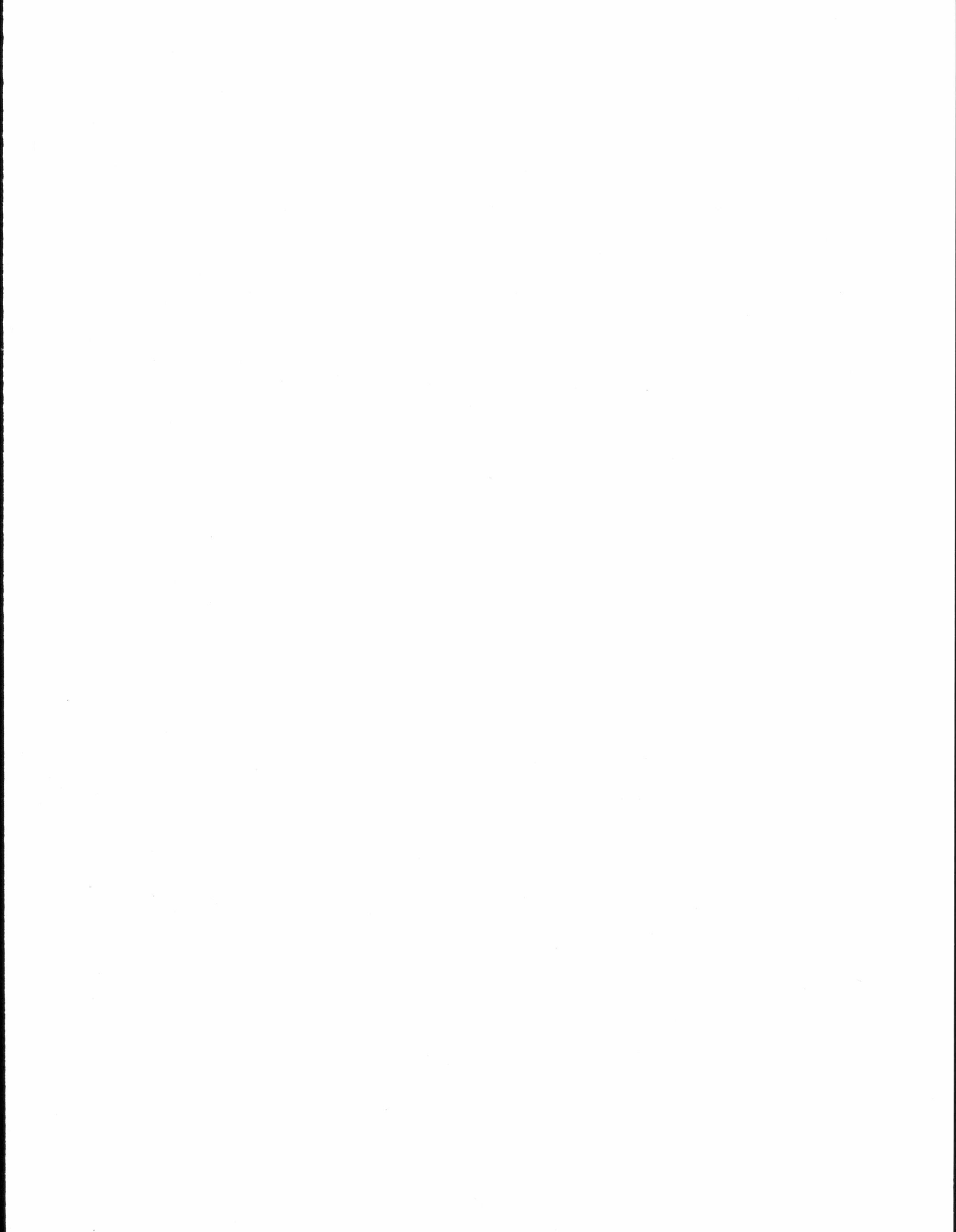


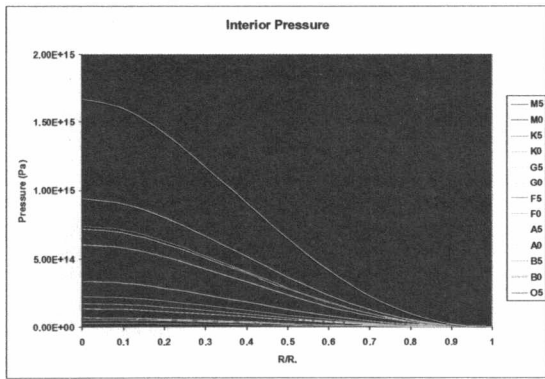
c)



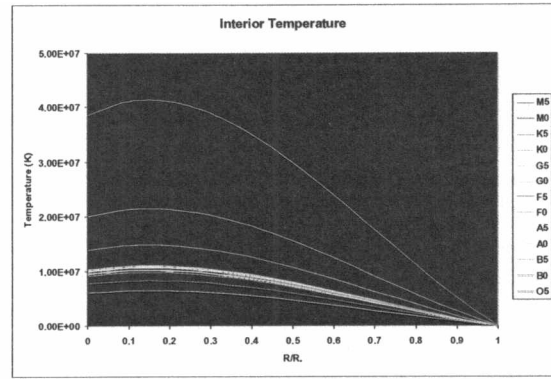
d)

Figure B1: a) core densities, b) pressures, c) temperatures, and d) total luminosities for each of the various main sequence spectral types.

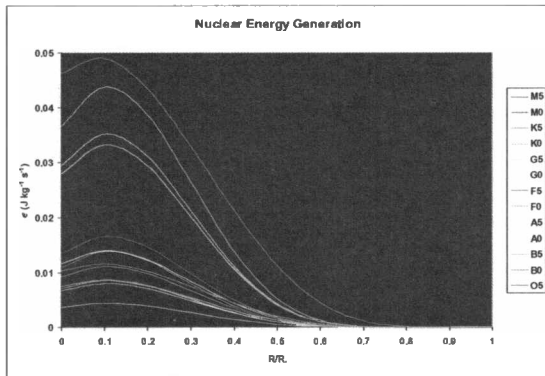




a)

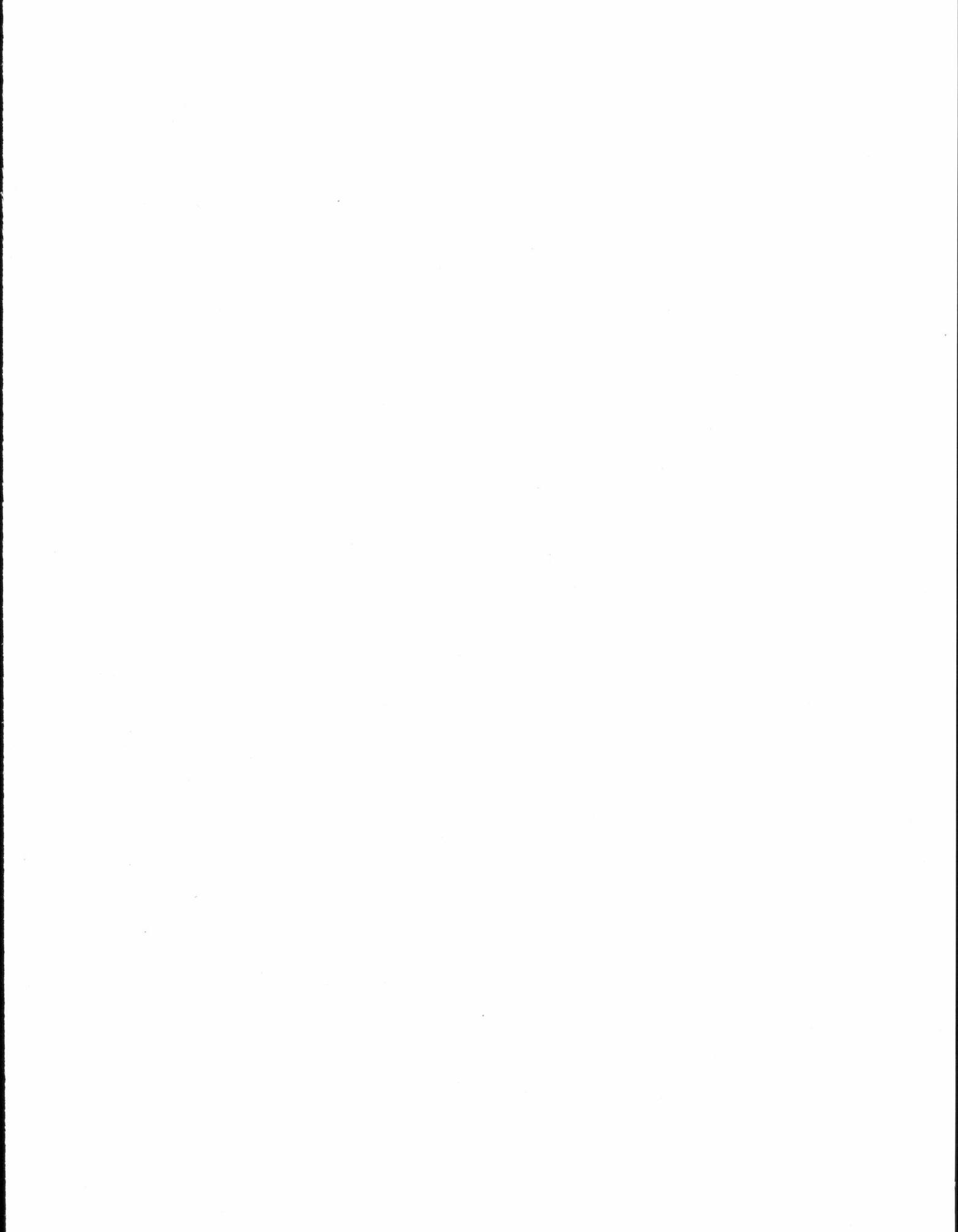


b)



c)

Figure B2: stellar interior structure for the linear density model.



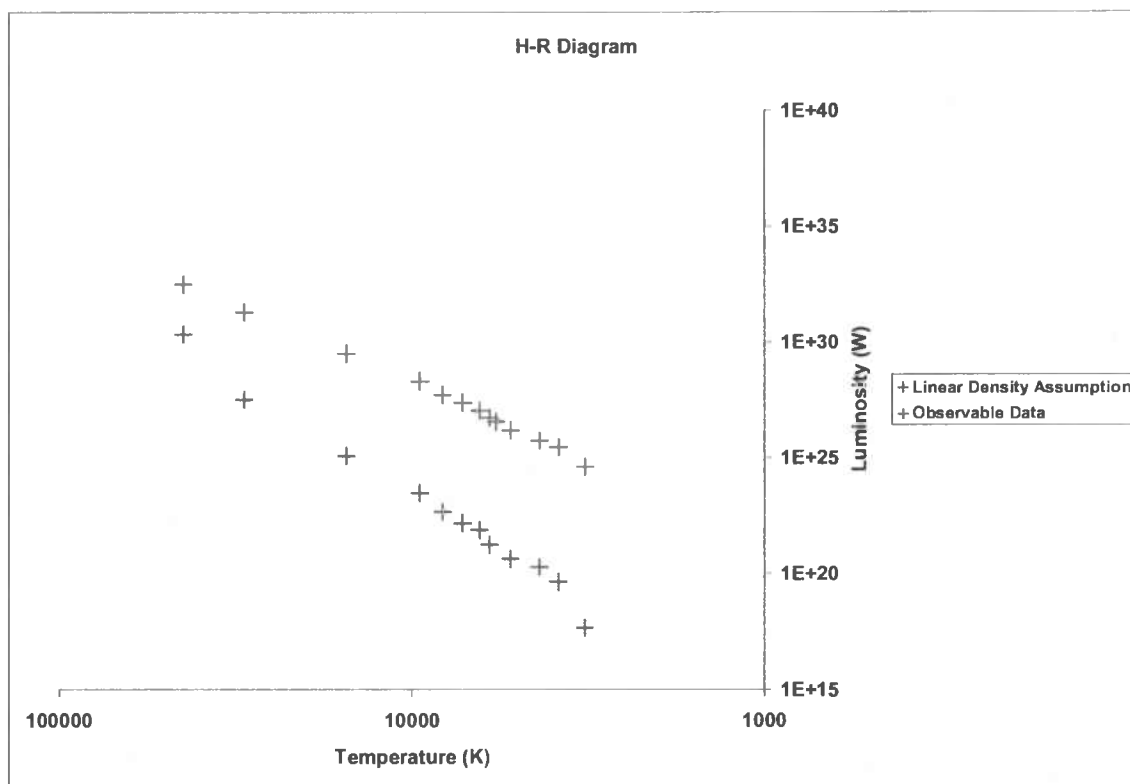
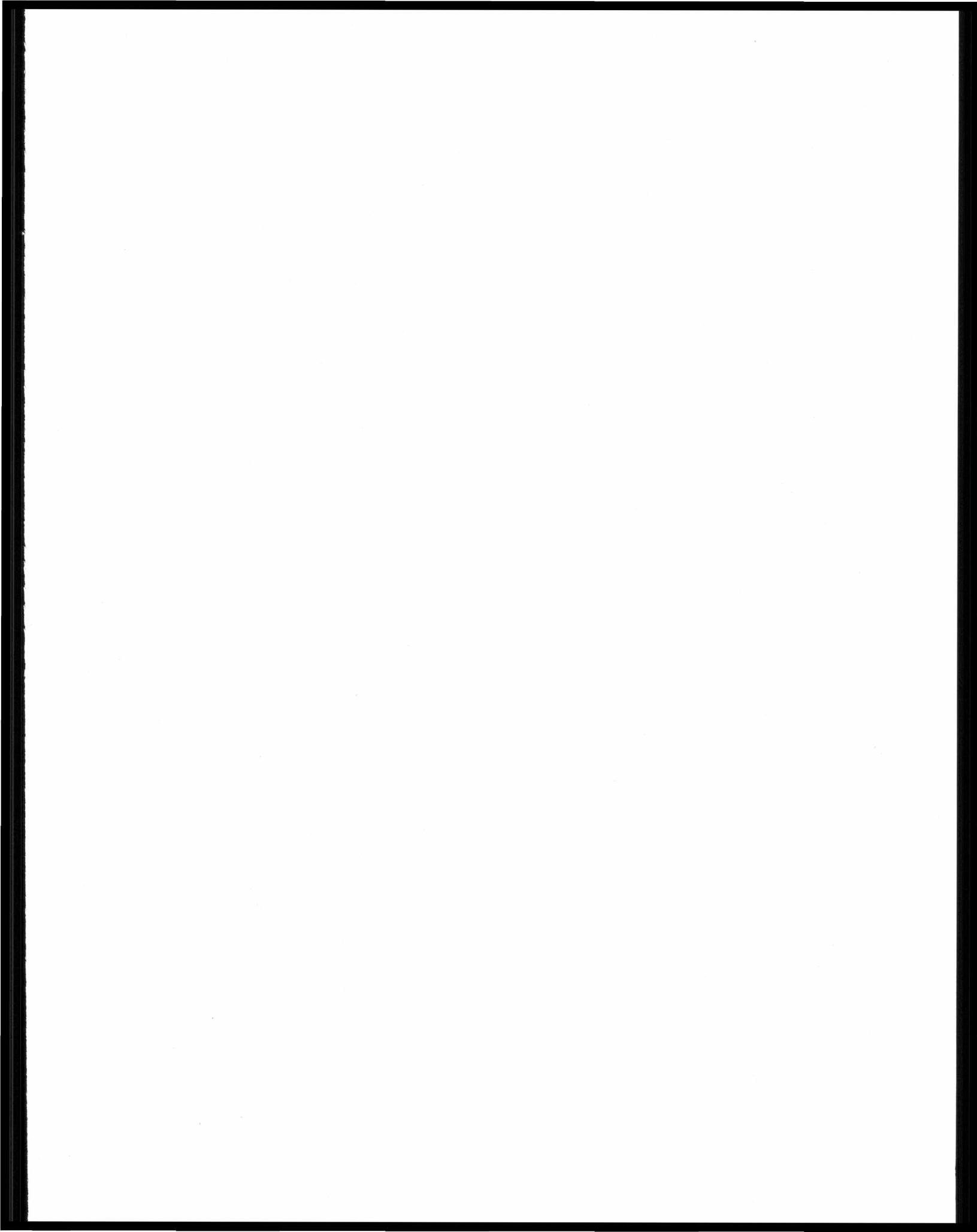


Figure B3: an H-R diagram comparing data from the linear density theoretical model with observable data.



WORKS CITED

Carroll, Bradley W., and Dale A. Ostlie. An Introduction to Modern Astrophysics.

Reading: Addison-Wesley Company, Inc, 1996. 255-373, A13-14.

Hansen, C. J., and S. D. Kawaler. Stellar Interiors - Physical Principles, Structure, and

Evolution. New York: Springer-Verlag New York, Inc, 1994. 1.

Watson, Dan. "Today in Astronomy 241: Model Stellar Interiors." University of

Rochester Physics & Astronomy. 22 Feb. 2005. University of Rochester. 22

Dec. 2006 <http://web1.pas.rochester.edu/~dmw/ast241/Classes/Class_12b.pdf>.

Zeilik, Michael, and Stephen A. Gregory. Introductory Astronomy & Astrophysics.

Fourth ed. Australia: Thomson Learning, Inc, 1998. 58-59.